We are IntechOpen,
the world's leading publisher of
Open Access books
Built by scientists, for scientists

6,900
Open access books available

186,000
International authors and editors

200M
Downloads

154
Countries delivered to

Our authors are among the

TOP 1%
most cited scientists

12.2%
Contributors from top 500 universities

BOOK CITATION INDEX
CLARIVATE ANALYTICS
INDEXED

WEB OF SCIENCE™

Selection of our books indexed in the Book Citation Index
in Web of Science™ Core Collection (BKCI)

Interested in publishing with us?
Contact book.department@intechopen.com

Numbers displayed above are based on latest data collected.
For more information visit www.intechopen.com

An Adaptive Two-Stage Observer in the Control of a New Electromagnetic Valve Actuator for Camless Internal Combustion Engines

Paolo Mercorelli
Ostfalia University of Applied Sciences, Faculty of Automotive Engineering
Robert Koch Platz 12, D-38440 Wolfsburg
Germany

1. Introduction

In this paper, the experimental results for the design and operation of a special linear electromagnetic motor as a variable engine valve actuator are presented. A detailed description is given on the design procedure aimed at meeting the requirements of a high dynamic range and low power consumption, including determinations of the actuator's topology and parameters, the force and the dynamic and power loss calculations. Moreover, based on a nonlinear model, an adaptive two-stage observer is presented to tackle unobservable points and achieve sensorless control. Further, this paper presents feasible real-time self-tuning of an approximated velocity estimator based on measurements of current and input voltage. The robustness of the velocity tracking is addressed using a minimum variance approach. The effect of the noise is minimised, and the position can be achieved through a two-stage structure between this particular velocity estimator and an observer based on the electromechanical system. This approach avoids a more complex structure for the observer and yields an acceptable performance and the elimination of bulky position-sensor systems. A control strategy is presented and discussed as well. Computer simulations of the sensorless control structure are presented in which the positive effects of the observer with optimised velocity are visible in the closed-loop control.

2. Background and state of the art

With the recent rapid progress in permanent-magnet technology, especially through the use of high-energy-density rare-earth materials, very compact and high-performance electromagnetic linear actuators are now available. They open new possibilities for high-force motion control in mechatronic applications, for which great flexibility, highly controlled dynamics and precise positioning are required at the same time. In the last years, variable engine valve control has attracted a lot of attention because of its ability to reduce pumping losses (work required to draw air into the cylinder under part-load operation) and to increase torque performance over a wider rage than conventional spark-ignition engines. Variable valve timing also allows the control of internal exhaust gas recirculation, thereby improving fuel economy and reducing NOx emissions. Besides mechanical and hydraulic variable valvetrain options, electromagnetic valve actuators have been reported in the past, see Refs.

(Ahmed & Theobald (1999)) and (Schlechter & Levin (1996)). Recent works mark technical progress in this area, in particular, Refs. (Tai & Tsao (2003)), (Hoffmann & Stefanopoulou (2001)) and (Peterson (2005)). Theoretically, electromagnetic valve actuators offer the highest potential to improve fuel economy due to their control flexibility. In real applications, however, the electromechanical valve actuators developed so far mostly suffer from high power consumption and other control problems. Therefore, innovative concepts are required to reduce the losses while keeping the actuator dynamic. In the first part of this paper, the theoretical and experimental results for the design of a novel permanent-magnet linear valve actuator are presented, allowing short-stroke high-dynamic operations combined with low power losses. In the second part of the paper, a sensorless control is shown. In such applications, sensorless control has always been a challenging problem when trying to avoid bulky position-sensor systems. To realise this goal, it is necessary to create an observer structure. The paper presents a two-stage observer. In particular, an approximated velocity observer is proposed. The parameters of this velocity observer are optimised using a technique similar to that presented in Ref. (Mercorelli (2009)). A second observer is considered, through measurement of the current and the velocity estimated by the first observer, to estimate the position of the valve. The paper is organised as follows. In Section 3, a new actuator design is shown. Section 4 is devoted to the analysis of the model. Next, an observability analysis is performed in Section 5. Section 6 shows the approximated velocity observer (first-stage) and its optimisation. Section 7 shows the design position observer (second-stage). In Section 8, a control strategy is presented and discussed. Section 9 presents computer simulations of the sensorless control structure, in which the positive effects of the optimised velocity observer are visible in the closed-loop control. The conclusions and future work close the paper.

3. Design specifications and actuator design

A sketch of an electromagnetic valve shaft is shown in the left part of Fig. 1 and its typical valve movement required by engine operation is show in the right part of Fig. 1. The variable stroke needed is between 0 and 8 mm and is to be realised within a time interval of about 4 ms. Thus, high accelerations up to $4,000\,\mathrm{m/s^2}$ have to be achieved, even in the case of large disturbances due to a strong cylinder pressure acting against the exhaust valve opening. For this reason, high forces coupled with a low moving mass are essential for actuator design. Furthermore, copper loss and the physical size of the actuator are also very important parameters to be considered.

Most electromechanical valve actuators reported so far are based on the principle of electromagnets see Refs. (Furlani (2001) & Butzmann et al. (2000)), utilising Maxwell attracting forces at both ends of the motion range. This operation principle is simple to implement, difficult to control and specifically lacks the ability to influence the valve motion in the middle range. Thus, variable opening strokes, which have recently been proven to be efficient for engine operation, are rarely possible. For this reason, we considered linear motors as valve actuators to allow for the ability to control the motion in the total range, including positioning the valve at every specified stroke. Due to the limited mounting space in the focused application, we chose perpendicularly formed linear motors. The actuator width was restricted to around 36 mm. As the main design goal was to have a high acceleration and low power loss at the same time, we used the following quality function Q as the design criterion to be minimised:
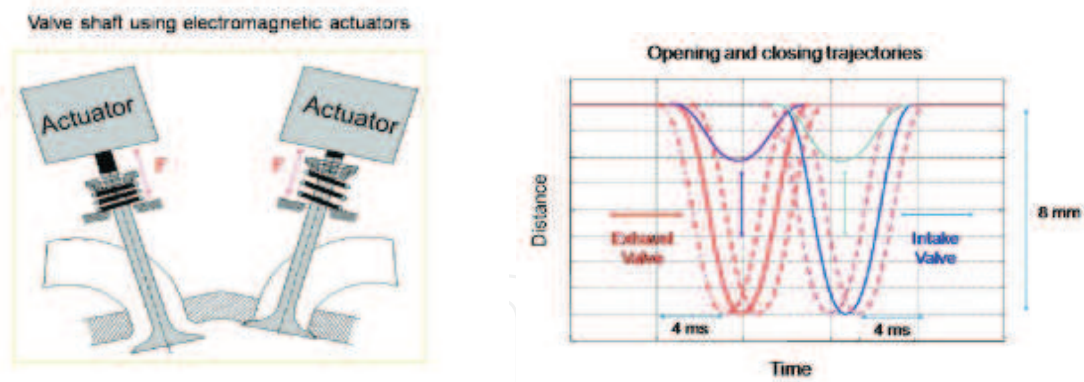
Fig. 1. Left: Electromagnetic actuators. Right: Opening and closing loop for valve operation

$$Q = \frac{P_v}{a} = \frac{P_v m}{F},\tag{1}$$

where P_v is the copper loss, a is the possible acceleration, m is the mass (moving part of the actuator and the valve), and F is the actuator force. Different permanent-magnet actuator topologies using NdFeB magnets were considered for the design. In this paper, we present a design study based on the following moving-magnet reluctance DC-actuator, whose basic element is shown in the left part of Fig. 2. One of the shortages of conventional linear motors in this application is the linear dependence between the desired force and the required current density (the Maxwell attracting force is quadratic to the current and inversely quadratic to the distance between the valve armature and the electromagnets). Thus, one needs high currents to generate high forces. Therefore, to reduce maximally the electrical power loss during normal valve operation, we use a spring oscillator supporting the periodic motion. The initial considerations for our actuator design are therefore based on a spring-mass system. The start and end positions of the system have high spring forces to give the moving part high accelerations. On the other hand, in conventional electromechanical valve actuators, it is usually necessary to have a constant hold current generating an electromagnetic force against the spring force at the end positions to keep the valve unmoved during the closed and opened phases (most of the time). This causes additional non-negligible power loss. In our design, we combine the linear motor with a reluctance armature using permanent magnets, such that the actuator can be kept at the end positions without a holding current. Furthermore, the reluctance force can be influenced by a coil current in such a way that a very high acceleration is possible. The principle topology of the novel-reluctance linear motor is depicted in the left part of Fig. 2. The stator of the actuator consists of a laminated iron core divided into two parts with a copper coil embedded in it. The armature sitting between the stator packages is built of thin permanent-magnet plates mechanically connected to each other. To produce a small moving mass, NdFeB magnets with a high energy density are used. Our basic idea is to utilise the position-dependent reluctance force to generate forces of different signs. In the case where the permanent magnets are in the position shown in the left part of Fig. 2 (valve closed), a magnetic flux is generated in the iron poles. This flux leads to a negative (i.e., valve opening) reluctance force in the y-direction without a current flowing in the coil. When the magnets are in the position at the opposite end, the same functional mechanism enables a reluctance force with a positive sign (valve opened). With an actively controlled current with different directions in the coils, it is possible to increase, reduce or reverse the
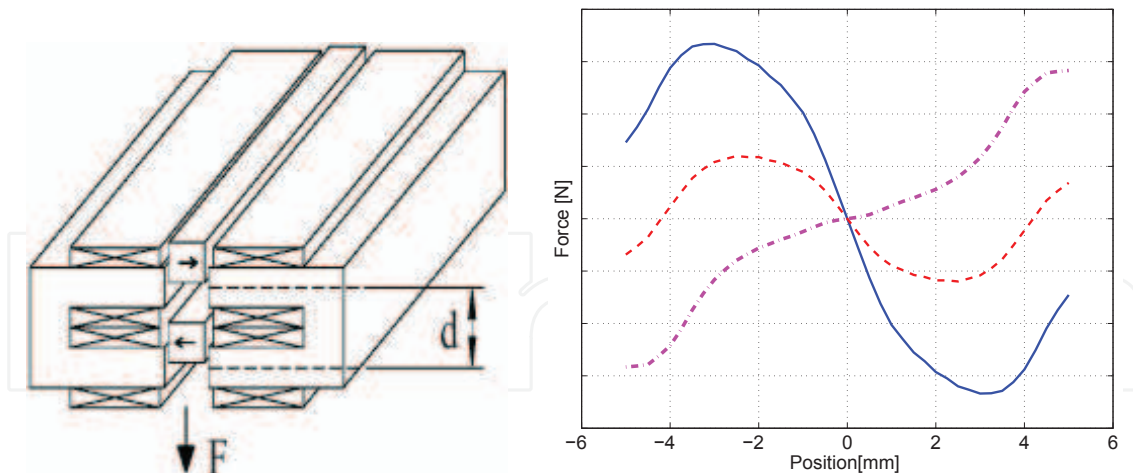
Fig. 2. Left: Basic element of the linear reluctance motor. Right: Calculated force depending of position and current (bl - neg. current, rd - no current, viol. - pos. current)

force. Obviously, this effect is determined by the geometry of the permanent magnets and iron poles with respect to each other and by the electrical current used. One important design criterion is the following. In the totally closed or opened valve position, the electromagnetic force (holding force) must be of the opposite sign and slightly stronger than the spring force to achieve low power consumption. In the right part of Fig. 2, the calculated position-dependent characteristics of the force generation using different current densities are presented. The calculation was
done using the finite-element tool ANSYS. It can be easily seen that if we put the holding position at -5 mm, there will be a reasonable negative holding force available. On the other hand, in the range of about -4 to -3 mm, a large acceleration force can be generated. Thus, by applying some suitable strategy, it is possible to combine both properties for an optimal motion. For this particular purpose, we designed a special system with separated hold and start positions for the valve. There are two different springs within the system: one valve spring connected with the valve shaft and one motor spring connected with the motor armature. They are identically built but have opposite unstressed points. In total, they act as a resulting spring in the motion range between 4 and -4 mm. After having seated the valve at 4 mm: however, the permanent-magnet armature with the motor spring continues to move to the hold position at 5 mm controlled by electronics. To open the valve, one must apply a proper current to release the motor from the hold position, travel to the top end of the valve shaft and make the valve move by generating the maximum reluctance force. In this way, the motor-spring system can be used at a very high efficiency, and an overall reduced power consumption can be achieved. Of course, a smooth motion is only possible using a sophisticated control strategy. The base element shown in the left part of Fig. 2 can be connected in series to obtain higher forces. Generally, due to the weight of the valve shaft, it is theoretically better to have more poles, enabling a higher acceleration. However, there are also tight limits for both the actuator volume and the material costs. We determined during our design process that some optimum can be reached using a four-pole or a six-pole topology. The left par of Fig. 3 shows such an actuator arrangement with its calculated force in position and current dependence depicted in the right part of Fig. 3. Clearly, combined with the spring, acceleration forces of 600 N or even larger values are possible. Such high forces are needed to open the exhaust valve against the gas pressure coming from the combustion chamber.
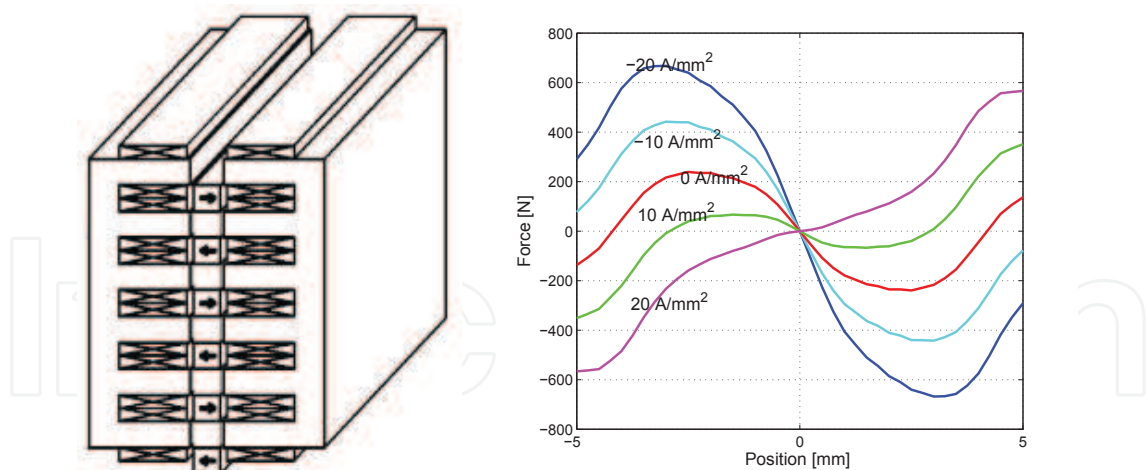
Fig. 3. Left: Actuator with 6 poles (valve position at $-4\,\mathrm{mm}$, i.e. in the opened position). Right: Reluctance force depending on position and current densities in a 6-pole motor (negative force - moving down).

Having determined the proper topology, we extensively used finite-element calculation to optimise the dimensions of the actuator. The actuator's outer width, height and depth are limited by the available mounting space and are very restrictive. The maximum width allowed is about 36 mm. Thus, subtracting the air gap of 0.5 mm on both sides of the armature, the remaining width is available for the stator and armature magnet systems. The operating point of the iron parts is defined to have a slight saturation, resulting in an effective use of the iron material and good performance. Based on these considerations, adjustments of the dimensions were made to ensure optimal operating points of the magnets and iron parts. While the actuator geometry parameters in the width direction are important for the reachable magnetic flux density in the air gaps, the parameters in the height are also essential for the form of the force curves (position dependence). One of the design goals is to have distinctive high forces using a negative current at the beginning of the valve opening phase (position $4 - 2\,\mathrm{mm}$)and, on the other hand, to obtain a reasonable holding force without current. This is because if there is a high gas pressure (some hundred Newtons) acting against the valve opening, it will decrease very rapidly after the opening phase has begun. Therefore, the higher the available reluctance force at the beginning, the faster the reduction of the gas

pressure that will follow, leading to a better motion dynamic and reduced copper loss. That is, we did not look for an as-constant-as-possible motor but for a nonlinear force curve adapted to the motion conditions. This is one of the special design aspects for the presented actuator. After having fixed some basic design parameters, the forces were calculated by finite-element calculation, and the quality function Q was evaluated to assess the performance. Subsequently, iterative calculations based on an optimisation strategy were carried out to optimise the design step-by-step, also taking into account the nonlinear saturation and leakage effects. As above mentioned, this optimisation procedure started using the finite-element tool ANSYS. In the left part of Fig. 4, a diagram used inside this optimization procedure excerpted from ANSYS program is shown. The iteration was also supported by dynamic simulations to determine the overall power loss during a total engine operation cycle at different speeds. For this purpose, a complex dynamic simulation model including the actuator, power electronics and simple control loops was developed and coupled with the FEM calculations. At the end of this process, a novel linear reluctance
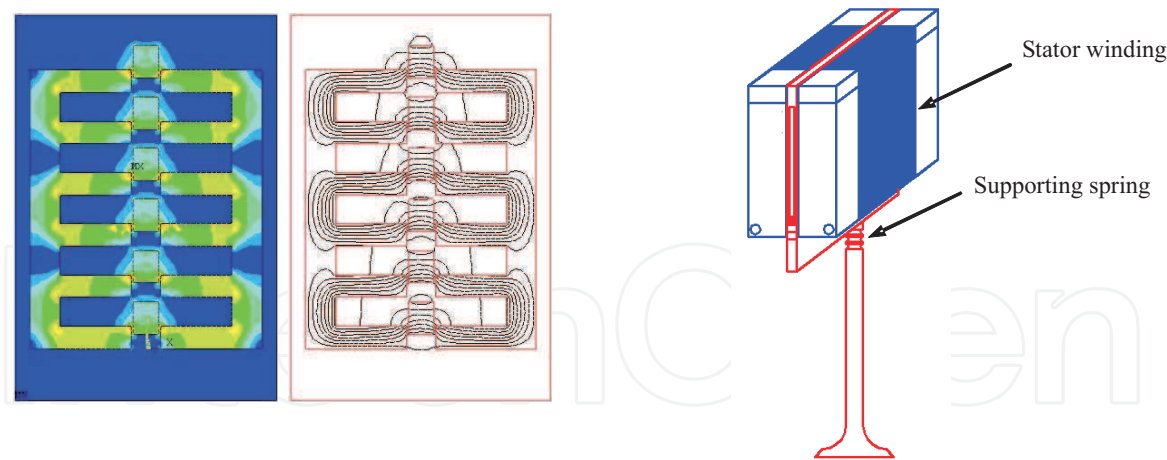
Fig. 4. Left: Flux density and magnetic field distribution (position 3mm, current density $-15\,\mathrm{A/mm^2}$). Right: Mechanical structure with valve coupling.

actuator with excellent dynamic parameters and low power losses was derived. The right part of Fig. 4 shows the mechanical structure of the actuator connected with the engine valve. In Table 1, some of the most interesting parameters of the developed actuator are given. It is easy to recognise that the specified technical characteristics were fully reached.

4. Description of the model

The electromagnetic actuator depicted in the left part of Fig. 3 can be modelled mathematically in the following way:

$$\frac{di_{\mathrm{Coil}}(t)}{dt} = -\frac{R_{\mathrm{Coil}}}{L_{\mathrm{Coil}}}i_{\mathrm{Coil}}(t) + \frac{u_{in}(t) - u_q(t)}{L_{\mathrm{Coil}}}, \tag{2}$$

$$\frac{dy(t)}{dt} = v(t), \tag{3}$$

Moving mass: (including an 50 g valve)	157 g
maximum opening force (for $-20\,\mathrm{A/mm^2}$)	625 N
maximum acceleration loss per acceleration quality function Q $\mathrm{Ws^2/m}$	3981 m/s^2 0.015
Dimensions: $W * H * D$ mm	36 * 61.5 *100
volume:	222 mm^3
magnet mass:	60 g
copper wire: stator iron package:	48 m (ca. 0.4 kg) 490 g

Table 1. Parameters of the actuator (6 poles)

$$\frac{dv(t)}{dt} = \frac{f(i_{\mathrm{Coil}}(t), y(t))}{m} i_{\mathrm{Coil}}(t) + \frac{-k_d v(t) - k_f y(t) + F_0(t)}{m}, \tag{4}$$

where

$$f(i_{Coil}(t), y(t)) = F_{lin}(y(t), i_{Coil}(t)) + F_{sin}(y(t), i_{Coil}(t)), \tag{5}$$

$$u_q(t) = k_1 \big(y(t) + sign(y(t)) k_2 \big) v(t), \tag{6}$$

and $\quad f(i_{Coil}(t), y(t)) = i_{Coil}(t) k_1 \big(y(t) + sign(y(t)) k_2 \big) + F_{sin}(y(t), i_{Coil}(t)), \tag{7}$

where k_1 and k_2 are physical constants. The non-linear electromagnetic force generation can be separated into two parallel blocks, $F_{sin}(y(t))$ and $F_{lin}(y(t), i_{Coil}(t))$, corresponding to the reluctance effect and the Lorentz force, respectively:

$$f(y(t), i_{Coil}(t)) = F_{sin}(y(t)) + F_{lin}(y(t), i_{Coil}(t)) \tag{8}$$

with the following approximation equations

$$F_{\sin}(y(t)) = F_{0,max} \sin(2\pi y(t)/d) \tag{9}$$

and $\quad F_{lin}(y(t), i_{Coil}(t)) = k_1 \big(y(t) + sign(y(t)) k_2 \big) i_{Coil}(t). \tag{10}$

R_{Coil} and L_{Coil} are the resistance and the inductance, respectively, of the coil windings, $u_{in}(t)$ is the input voltage and $u_q(t)$ is the induced emf. $i_{Coil}(t)$, $y(t)$, $v(t)$ and m are the coil current, position, velocity and mass of the actuator respectively, while $k_d v(t)$, $k_f y(t)$ and $F_0(t)$ represent the viscose friction, the total spring force and the disturbance force acting on the valve, respectively.

5. Observability analysis

Definition 1 *Given the following nonlinear system:*

$$\dot{\mathbf{x}}(t) = \mathbf{f}(\mathbf{x}(t)) + \mathbf{g}(\mathbf{x}(t)) \mathbf{u}(t) \tag{11}$$

$$\mathbf{y}(t) = \mathbf{h}(\mathbf{x}(t)), \tag{12}$$

where $\mathbf{x}(t) \in \Re^n$, $\mathbf{u}(t) \in \Re^m$, and $\mathbf{y} \in \Re^p$, a system in the form of Eqs. (11) and (12) is said to be locally observable at a point $\mathbf{x}_0$ if all states $x(t)$ can be instantaneously distinguished by a judicious choice of input $\mathbf{u}(t)$ in a neighbourhood $\mathbf{U}$ of $\mathbf{x}_0$ (Hermann & Krener (1997)), (Kwatny & Chang (2005)). ☐

Definition 2 *For a vector $\mathbf{x} \in \Re^n$, a real-valued function $\mathbf{h}(\mathbf{x}(t))$, which is the derivative of $h(\mathbf{x}(t))$ along $\mathbf{f}$ according to Ref. (Slotine (1991)) is denoted by*

$$L_{\mathbf{f}} \mathbf{h}(\mathbf{x}(t)) = \sum_{i=1}^{n} \frac{d\mathbf{h}(\mathbf{x}(t))}{d\mathbf{x}_i(t)} \mathbf{f}_i(\mathbf{x}(t)) = \frac{d\mathbf{h}(\mathbf{x}(t))}{d\mathbf{x}(t)} \mathbf{f}(\mathbf{x}(t)).$$

Function $L_{\mathbf{f}}\mathbf{h}(\mathbf{x}(t))$ represents the derivative of $\mathbf{h}$ first along a vector field $\mathbf{f}(\mathbf{x}(t))$. Function $L_{\mathbf{f}}^i\mathbf{h}(\mathbf{x}(t))$
satisfies the recursion relation

$$dL_{\mathbf{f}}^i\mathbf{h}(\mathbf{x}(t)) = \frac{dL_{\mathbf{f}}^{i-1}\mathbf{h}(\mathbf{x}(t))}{d\mathbf{x}(t)}\mathbf{f}(\mathbf{x}(t)) \tag{13}$$

with $L_{\mathbf{f}}^0\mathbf{h}(\mathbf{x}(t)) = \mathbf{h}(\mathbf{x}(t))$.   □

Test criteria can be derived according to the local observability definitions (Hermann & Krener (1997)), (Kwatny & Chang (2005)). In particular, if $\mathbf{u}(t) = 0$ the system is called "*zero input observable*," which is also important for this application because if a system is zero input observable, then it is also locally observable (Xia & Zeitz (1997)). In fact, the author in Ref. Fabbrini et al. (2008) showed how an optimal trajectory, derived from a minimum power consumption criterion, is achieved by an input voltage that is zero or very close to zero for some finite time intervals.

Rank Condition 1 *The system described in Eqs. (11) and (12) is autonomous if $\mathbf{u}(t) = 0$. The following rank condition (Hermann & Krener (1997)), (Kwatny & Chang (2005)) is used to determine the local observability for the nonlinear system stated in Eq. (11). The system is locally observable if and only if*

$$\mathsf{dim}\big(O(\mathbf{x}_0)\big) = \frac{dl(\mathbf{x}(t))}{d\mathbf{x}(t)}\Big|_{\mathbf{x}_0} = n, \text{where } l(\mathbf{x}(t)) = \left[\begin{array}{c} L_{\mathbf{f}}^0(\mathbf{h}(\mathbf{x}(t))) \\ L_{\mathbf{f}}(\mathbf{h}(\mathbf{x}(t))) \\ L_{\mathbf{f}}^2(\mathbf{h}(\mathbf{x}(t))) \end{array}\right].$$

□

Applying the above criterion with $\mathbf{x}(t) = \left[\begin{array}{c} i_{Coil}(t) \\ y(t) \\ v(t) \end{array}\right]$ and $\mathbf{h}(\mathbf{x}(t)) = i_{Coil}(t)$, then

$$dL_{\mathbf{f}}^0\mathbf{h}(\mathbf{x}(t)) = \frac{d\mathbf{h}}{d\mathbf{x}(t)} = \begin{pmatrix} 1 & 0 & 0 \end{pmatrix}, \tag{14}$$

$$L_{\mathbf{f}}\mathbf{h}(\mathbf{x}(t)) = -\frac{R_{Coil}}{L_{Coil}}I_{Coil}(t) - \frac{u_q(t)}{L_{Coil}}, \tag{15}$$

$$dL_{\mathbf{f}}\mathbf{h}(\mathbf{x}(t)) = \frac{1}{L_{\text{Coil}}}\left[-R_C \quad -\frac{du_q(t)}{dy(t)} \quad -\frac{du_q(t)}{dv(t)}\right], \tag{16}$$

where

$$\frac{du_q(t)}{dy(t)} = k_1 v(t)$$

and

$$\frac{du_q(t)}{dv(t)} = k_1\big(y(t) + sign(y(t))k_2\big).$$

According to the definition in Eq. (2), then

$$L_{\mathbf{f}}^2\mathbf{h}(\mathbf{x}(t)) = \frac{dL_{\mathbf{f}}\mathbf{h}(\mathbf{x}(t))}{d\mathbf{x}(t)}\mathbf{f}(\mathbf{x}(t)),$$

An AdaptiveyTwo-Stage Observer in the Control of a
New Electromagnetic Valve Actuator for Camless Internal Combustion Engines

351

$$\frac{dL_{\mathbf{f}}\mathbf{h}(\mathbf{x}(t))}{d\mathbf{x}(t)}\mathbf{f}(\mathbf{x}(t)) = -\frac{1}{L_{Coil}}\left(R_{Coil}\left(-\frac{R_{Coil}}{L_{Coil}}I_{Coil}(t) - \frac{u_q(t)}{L_{Coil}}\right) + \frac{du_q(t)}{dy(t)}v(t) + \frac{du_q(t)}{dv(t)}\frac{dv(t)}{dt}\right).$$
(17)

For the sake of notation,

$$dL_{\mathbf{f}}^2\mathbf{h}(\mathbf{x}(t)) = \begin{bmatrix} M_1(t) & M_2(t) & M_3(t) \end{bmatrix},$$

where $M_1(t)$, $M_2(t)$ and $M_3(t)$ are functions of the variables $i_{Coil}(t)$, $y(t)$ and $v(t)$. In particular, it is useful to note that the term

$$M_2(t) = \frac{R_{Col}}{L_{Coil}^2}\frac{du_q(t)}{dy(t)} - \frac{1}{L_{Coil}}\left(\frac{d^2u_q(t)}{dy(t)^2}v(t) + \frac{du_q(t)}{dy(t)}v(t) + \right.$$

$$\left. \frac{d}{dy(t)}\left(\frac{du_q(t)}{dv(t)}\right)\frac{dv(t)}{dt} + \frac{du_q(t)}{dv(t)}\frac{d}{dy(t)}\left(\frac{dv(t)}{dt}\right)\right) \quad (18)$$

and

$$M_3(t) = \frac{R_{Coil}}{L_{Coil}^2}\frac{du_q(t)}{dv(t)} + \frac{2}{L_{Coil}^2}\frac{F_{0,max}\pi}{d}\cos\left(\frac{\pi y(t)}{d}\right)v(t) + \frac{du_q(t)}{dv(t)}\frac{d}{dv(t)}\left(\frac{dv(t)}{dt}\right). \quad (19)$$

Matrix $O(\mathbf{x}_0)$ becomes

$$O(\mathbf{x}_0) = \begin{bmatrix} 1 & 0 & 0 \\ -R_C & -\frac{du_q(t)}{dy(t)} & -\frac{du_q(t)}{dv(t)} \\ M_1(t) & M_2(t) & M_3(t) \end{bmatrix}. \quad (20)$$

If set $\mathbf{x}_0 = \{v(t) = 0, y(t) = 0\}$ is considered, then matrix (20) has not full rank. In fact, being $\frac{du_q(t)}{dv(t)} = k_1\left(y(t) + sign(y(t))k_2\right)$, then $\frac{du_q(t)}{dv(t)}|_{\mathbf{x}_0} = 0$; considering Eq. (19) calculated in $\mathbf{x}_0$, it follows that $M_3(t) = 0$. So it is shown that the third column of matrix (20) is equal to zero, thus matrix (20) has not full rank.

If set $\mathbf{x}_1 = \{v(t) = 0\}$ is considered, then matrix (20) has not full rank. In fact, being $\frac{du_q(t)}{dy(t)} = k_1 v(t)$, then $\frac{du_q(t)}{dy(t)}|_{\mathbf{x}_1} = 0$; if $y(t) \neq 0$, then also $\frac{dv(t)}{dt} = 0$ and considering Eq. (18) calculated in $\mathbf{x}_1$, it follows that $M_2(t)|_{\mathbf{x}_1} = 0$. So it is shown that the three rows of matrix (20) are linearly dependent, and thus matrix (20) has not full rank.

Rank Condition 2 *The system described in (11) and (12) is not autonomous if $\mathbf{u}(t) \neq 0$. The following condition (Hermann & Krener (1997)), (Kwatny & Chang (2005)) is used to determine the local observability for the nonlinear system stated in (11). The system is locally observable if and only if*

$$\dim\left(O(\mathbf{x}_0)\right) = \frac{dl(\mathbf{x}(t))}{d\mathbf{x}(t)}\bigg|_{\mathbf{x}_0} = n, \text{ where } l(\mathbf{x}(t)) = \begin{bmatrix} L_{\mathbf{f}}^0(\mathbf{h}(\mathbf{x}(t))) \\ L_{\mathbf{f}}(\mathbf{h}(\mathbf{x}(t))) \\ L_{\mathbf{f}}^2(\mathbf{h}(\mathbf{x}(t))) \\ L_{\mathbf{g}}L_{\mathbf{f}}(\mathbf{h}(\mathbf{x}(t))) \end{bmatrix}. \qquad \square$$

It is to note that $L_{\mathbf{g}}L_{\mathbf{f}}(\mathbf{h}(\mathbf{x}(t))) = -\frac{R_{Coil}}{L_{Coil}^2}$ and that $dL_{\mathbf{g}}L_{\mathbf{f}}(\mathbf{h}(\mathbf{x}(t))) = [0 \quad 0 \quad 0]$. This means that, even for a *judicious choice* of input $\mathbf{u}(t)$, no contribution to the observability set is given if compared with the autonomous case provided above. The rank criteria provide sufficient and necessary conditions for the observability of a nonlinear system. Moreover, for applications it is useful to detect those sets where the *observability level* of the state variables decreases; thus, a measurement of the observability is sometimes needed. A heuristic criterion for testing the level of unobservability of such a system is to check where the *signal connection* between the mechanical and electrical system decreases or goes to zero. Although this criterion does not guarantee any conclusions about observability, it could be useful in an initial analysis of the system. In fact, it is well-known that the observability is an analytic concept connected with the concept of distinguishability. In the present case, the following two terms,

$$u_q(t) = k_1(y(t) + sign(y(t))k_2)v(t) \quad \text{and} \quad \mathbf{f}(i_{Coil}(t), y(t))$$

are responsible for the feedback mentioned above. If the term $u_q(t) \to 0$, and $\mathbf{f}(i_{Coil}(t), y(t)) \neq 0$ when $v(t) \to 0$, then the above tests result in unobservability. In fact, as Eq. (4) for $v(t) \to 0$ is satisfied by more than one point position $y(t)$, this yields the indistinguishability of the states and thus the unobservability. If $y(t) \to 0$, it is noticed that both terms $u_q(t) \to 0$ and $\mathbf{f}(i_{Coil}(t), y(t)) \to 0$; nevertheless, Eq. (4) is unequivocally satisfied and this yields observability. However, the "level of observability," if an observability function is defined and calculated, decreases. In fact, if the observability is calculated as a function at this point, it assumes a minimum.

The *unobservable sets* should be avoided in the observer design; thus, a thorough analysis of the observability is important. Sensorless operations tend to perform poorly in low-speed environments, as nonlinear observer-based algorithms work only if the rotor speed is high enough. In low-speed regions, an open loop control strategy must be considered. One of the first attempts to develop an open loop observer for a permanent motor drive is described in Ref. (Wu & Slemon (1991)). In a more recent work (Zhu et al (2001)), the authors proposed a nonlinear-state observer for the sensorless control of a permanent-magnet AC machine, based to a great extent on the work described in Refs. (Rajamani (1998)) and (Thau (1973)). The approach presented in Refs. (Rajamani (1998)) and (Thau (1973)) consists of an observable linear system and a Lipschitz nonlinear part. The observer is basically a Luenenberger observer, in which the gain is calculated through a Lyapunov approach. In Ref. (Zhu et al (2001)), the authors used a change of variables to obtain a nonlinear system consisting of an observable linear part and a Lipschitz nonlinear part. In the work presented here, our system does not satisfy the condition in Ref. (Thau (1973)); thus, a Luenenberger observer is not feasible.

6. First-stage of the state observer design: open loop velocity observer

As discussed above, the proposed technique avoids a more complex non-linear observer, as proposed in Refs. (Dagci et al. (2002)) and (Beghi et al. (2006)). A two-stage structure is used for the estimation. An approximated open loop velocity observer is built from equation 2; then, a second observer is considered which, through the measurement of the current and the velocity estimated by the first observer, estimates the position of the valve. This technique avoids the need for a complete observer. If the electrical part of the system is considered, then

$$\frac{di_{\text{Coil}}(t)}{dt} = -\frac{R_{\text{Coil}}}{L_{\text{Coil}}} i_{\text{Coil}}(t) + \frac{u_{in}(t) - C\phi(i_{\text{Coil}}(t), y(t))v(t)}{L_{\text{Coil}}}; \tag{21}$$

considering that $C\phi(y(t)) = k_1(y(t) + sign(y(t))k_2$, and that if $y(t) = 0 \to sign(y(t)) = +1$, then $\forall\, y(t)\; C\phi(y(t)) = k_1(y(t) + sign(y(t))k_2 \neq 0$, it is possible to write that

$$v(t) = -\frac{L_{\text{Coil}}\frac{di_{\text{Coil}}(t)}{dt} + R_{\text{Coil}}i_{\text{Coil}}(t) - u_{in}(t)}{C\phi(y(t))}. \tag{22}$$

Consider the following dynamic system

$$\frac{d\hat{v}(t)}{dt} = -\mathcal{K}\hat{v}(t) - \mathcal{K}\frac{k_{di}L_{\text{Coil}}\frac{di_{\text{Coil}}(t)}{dt} + k_{pi}R_{\text{Coil}}i_{\text{Coil}}(t) - k_{pu}u_{in}(t)}{C\phi(y(t))}, \tag{23}$$

where $\mathcal{K}$, k_{di}, k_{pi} and k_{pu} are functions to be calculated. If the error on the velocity is defined as the difference between the true and the observed velocity, then:

$$e_v(t) = v(t) - \hat{v}(t) \tag{24}$$

and

$$\frac{de_v(t)}{dt} = \frac{dv(t)}{dt} - \frac{d\hat{v}(t)}{dt}. \tag{25}$$

If the following assumption is given:

$$\left\|\frac{dv(t)}{dt}\right\| << \left\|\frac{d\hat{v}(t)}{dt}\right\|, \tag{26}$$

then in Eq. (25), the term $\frac{dv(t)}{dt}$ is negligible. Using equation (23), Eq. (25) becomes

$$\frac{de_v(t)}{dt} = \mathcal{K}\hat{v}(t) + \mathcal{K}\frac{k_{di}L_{\text{Coil}}\frac{di_{\text{Coil}}(t)}{dt} + k_{pi}R_{\text{Coil}}i_{\text{Coil}}(t) - k_{pu}u_{in}(t)}{C\phi(y(t))}. \tag{27}$$

Remark 1 *Assumption (26) states that the dynamics of the approximating observer should be faster than the dynamics of the physical system. This assumption is typical for the design of observers.* □

Because of Eq. (22), (27) can be written as follows:

$$\frac{de_v(t)}{dt} = \mathcal{K}\hat{v}(t) - \mathcal{K}v(t)$$

and considering (24), then

$$\frac{de_v(t)}{dt} + \mathcal{K}e_v(t) = 0 \tag{28}$$

$\mathcal{K}$ can be chosen to make Eq. (28) exponentially stable. To guarantee exponential stability, $\mathcal{K}$ must be

$$\mathcal{K} > 0.$$

To guarantee $\|\frac{dv(t)}{dt}\| << \|\frac{d\hat{v}(t)}{dt}\|$, then $\mathcal{K} >> 0$. The observer defined in (23) suffers from the presence of the derivative of the measured current. In fact, if measurement noise is present in the measured current, then undesirable spikes are generated by the differentiation. The proposed algorithm needs to cancel the contribution from the measured current derivative. This is possible by correcting the observed velocity with a function of the measured current, using a supplementary variable defined as

$$\eta(t) = \hat{v}(t) + \mathcal{N}(i_{\text{Coil}}(t)), \tag{29}$$

where $\mathcal{N}(i_{\text{Coil}}(t))$ is the function to be designed.
Consider

$$\frac{d\eta(t)}{dt} = \frac{d\hat{v}(t)}{dt} + \frac{d\mathcal{N}(i_{\text{Coil}}(t))}{dt} \tag{30}$$

and let

$$\frac{d\mathcal{N}(i_{\text{Coil}}(t))}{dt} = \frac{d\mathcal{N}(i_{\text{Coil}}(t))}{di_{\text{Coil}}(t)} \frac{di_{\text{Coil}}(t)}{dt} = \mathcal{K}\frac{k_{di}L_{Coil}}{C\phi(y(t))}\frac{di_{\text{Coil}}(t)}{dt}. \tag{31}$$

The purpose of (31) is to cancel the differential contribution from (23). In fact, (29) and (30) yield, respectively,

$$\hat{v}(t) = \eta(t) - \mathcal{N}(i_{\text{Coil}}(t)) \quad \text{and} \tag{32}$$

$$\frac{d\hat{v}(t)}{dt} = \frac{d\eta(t)}{dt} - \frac{d\mathcal{N}(i_{\text{Coil}}(t))}{dt}. \tag{33}$$

Substituting (31) in (33) results in

$$\frac{d\hat{v}(t)}{dt} = \frac{d\eta(t)}{dt} - \mathcal{K}\frac{k_{di}L_{Coil}}{C\phi(y(t))}\frac{di_{\text{Coil}}(t)}{dt}. \tag{34}$$

Inserting Eq. (34) into Eq. (23) the following expression is obtained[1]:

$$\frac{d\eta(t)}{dt} - \mathcal{K}\frac{k_{di}L_{Coil}}{C\phi(y(t))}\frac{di_{\text{Coil}}(t)}{dt} = -\mathcal{K}\hat{v}(t) - \\ \mathcal{K}\frac{k_{di}L_{Coil}\frac{di_{\text{Coil}}(t)}{dt} + k_{pi}R_{\text{Coil}}i_{\text{Coil}}(t) - k_{pu}u_{in}(t)}{C\phi(y(t))}; \tag{35}$$

then

$$\frac{d\eta(t)}{dt} = -\mathcal{K}\hat{v}(t) - \mathcal{K}\frac{k_{pi}R_{\text{Coil}}i_{\text{Coil}}(t) - k_{pu}u_{in}(t)}{C\phi(y(t))}. \tag{36}$$

Letting $\mathcal{N}(i_{\text{Coil}}(t)) = k_{app}i_{\text{Coil}}(t)$, where with k_{app} a parameter has been indicated, then, from (31) $\Rightarrow \mathcal{K} = \frac{k_{app}}{k_{di}L_{Coil}}C\phi(y(t))$, Eq. (32) becomes

$$\hat{v}(t) = \eta(t) - k_{app}i_{\text{Coil}}(t). \tag{37}$$

---

[1]Expression (23) works under the assumption (26): fast observer dynamics.

Finally, substituting (37) into (36) results in the following equation

$$\frac{d\eta(t)}{dt} = -\frac{k_{app}}{k_{di}L_{Coil}} C\phi(y(t)) \left(\eta(t) - k_{app}i_{Coil}(t) \right) +$$

$$\frac{k_{app}C\phi(y(t))}{k_{di}L_{Coil}} \left(k_{pu}u_{in}(t) - k_{pi}R_{Coil}i_{Coil}(t) \right) \quad (38)$$

$$\hat{v}(t) = \eta(t) - k_{app}i_{Coil}(t). \quad (39)$$

Remark 2 *If $y(t) > 0$, then $C\phi(y(t)) > 0$, condition $\lim_{t\to\infty} e_v(t) = v(t) - \hat{v}(t) = 0$ is always guaranteed for $k_{app} > 0$. In fact, under condition (26), the system described in (39) satisfies condition (28) by construction. If $y(t) \le 0$, then $C\phi(y(t)) < 0$, $\lim_{t\to\infty} e_v(t) = v(t) - \hat{v}(t) = 0$ is always guaranteed for $k_{app} < 0$.* $\square$

Using the implicit Euler method, then the following velocity observer structure is obtained:

$$\eta(k) = \frac{\eta(k-1)}{1 + t_s \frac{k_{app}C\phi(y(k))}{k_{di}L_{Coil}}} + \frac{t_s \frac{k_{app}^2 C\phi(y(k))}{k_{di}L_{Coil}} - \frac{t_s k_{pi}R_{Coil}k_{app}C\phi(y(k))}{k_{di}L_{Coil}}}{1 + t_s \frac{k_{app}C\phi(y(k))}{k_{di}L_{Coil}}} i_{Coil}(k) +$$

$$\frac{t_s \frac{k_{app}C\phi(y(k))}{k_{di}L_{Coil}}k_{pu}}{1 + t_s \frac{k_{app}C\phi(y(k))}{k_{di}L_{Coil}}} u_{in}(k) \quad (40)$$

$$\hat{v}(k) = \eta(k) - k_{app}i_{Coil}(k), \quad (41)$$

where t_s is the sampling period. The digital asymptotic convergence that can be expressed by $\lim_{k\to\infty} e_v(k) = v(k) - \hat{v}(k) = 0$ is guaranteed for $k_{app} > 0$.

Remark 3 *A more useful case for the presented application is where the asymptotic convergence is oscillatory. If the transfer function of (41) is considered, to realize an oscillatory asymptotic convergence, it is necessary that the denominator in (41) must be*

$$(1 + t_s \frac{k_{app}}{k_{di}L_{Coil}}) < -1,$$

as in Ref. (Franklin et al. (1997)). In fact, the denominator in (41) must be < -1. Then,

$$k_{app} < -2\frac{k_{di}L_{Coil}}{t_s}. \quad (42)$$

Condition (42) is important in the structure of the presented approach. In fact, the proposed observer originates through the assumption

$$\|\frac{dv(t)}{dt}\| << \|\frac{d\hat{v}(t)}{dt}\|. \quad (43)$$

To achieve this condition, it is helpful to combine oscillations of $\hat{v}(t)$ with the high speed dynamics of the observer. High speed dynamics is obtained with a relative large value of the parameter $\|k_{app}\|$. $\square$

State variable $y(k)$ has a slow dynamics if it is compared with the other state ones. For that, $y(k)$ can be considered as a parameter. Transforming the velocity observer represented in (40) and (41) with the Z-transform, then the following equations are obtained:

$$\hat{V}(z) = \frac{t_s \frac{k_{app}C\phi(y(k))}{k_{di}L_{Coil}}(-k_{pi}R_{Coil} + k_{app})}{1 + t_s \frac{k_{app}}{k_{di}L_{Coil}}C\phi(y(k)) - z^{-1}}I_{Coil}(z)$$

$$+ \frac{t_s \frac{k_{app}C\phi(y(k))}{k_{di}L_{Coil}}k_{pu}}{1 + t_s \frac{k_{app}}{k_{di}L_{Coil}}C\phi(y(k)) - z^{-1}}U_{in}(z) - k_{app}I_{Coil}(z), \quad (44)$$

and

$$\hat{V}(z) = \frac{-k_{app} + k_{app}z^{-1} - t_s \frac{k_{app}C\phi(y(k))}{k_{di}L_{Coil}}k_{pi}R_{Coil}}{1 + t_s \frac{k_{app}}{k_{di}L_{Coil}}C\phi(y(k)) - z^{-1}}I_{Coil}(z)$$

$$+ \frac{t_s \frac{k_{app}C\phi(y(k))}{k_{di}L_{Coil}}k_{pu}}{1 + t_s \frac{k_{app}}{k_{di}L_{Coil}}C\phi(y(k)) - z^{-1}}U_{in}(z). \quad (45)$$

6.1 Optimal choice of the observer parameters: real-time self-tuning

Parameters k_{app}, k_{pi}, k_{di} and k_{pu} are now optimised using an algorithm similar to that presented in Ref. (Mercorelli (2009)). As described earlier, the objective of the minimum variance control is to minimise the variation in the system output with respect to a desired output signal, in the presence of noise. This is an optimisation algorithm, i.e., the discrete $\hat{v}(k)$ is chosen to minimise

$$J = E\{e_v^2(k+d)\},$$

where $e_v = v(k) - \hat{v}(k)$ is the estimation velocity error, d is the delay time, and E is the expected value. It should be noted that the velocity observer described in Eq. (45) has a relative degree equal to zero, and that the plant can be approximated with a two-order system. In fact, the electrical dynamics is much faster than the mechanical dynamics. Considering

$$\hat{V}_i(z) = \frac{-k_{app} + k_{app}z^{-1} - t_s \frac{k_{app}C\phi(y(k))}{k_{di}L_{Coil}}k_{pi}R_{Coil}}{1 + t_s \frac{k_{app}}{k_{di}L_{Coil}}C\phi(y(k)) - z^{-1}}I_{Coil}(z) \quad (46)$$

and

$$\hat{V}_u(z) = \frac{t_s \frac{k_{app}C\phi(y(k))}{k_{di}L_{Coil}}k_{pu}}{1 + t_s \frac{k_{app}}{k_{di}L_{Coil}}C\phi(y(k)) - z^{-1}}U_{in}(z), \quad (47)$$

it is obtained that:

$$\hat{V}(z) = \hat{V}_i(z) + \hat{V}_u(z). \quad (48)$$

Considering the estimated velocity signal $\hat{v}_i(t)$ due to the current input and with $u_{in}(t) = 0$, then it is possible to assume an ARMAX model as follows:

$$v_i(k) = \hat{v}_i(k) + a_{1i}\hat{v}_i(k-1) + a_{2i}\hat{v}_i(k-2) + b_{1i}i_{Coil}(k-1) + b_{2i}i_{Coil}(k-2)$$
$$+ n(k) + c_{1i}n(k-1) + c_{2i}n(k-2), \quad (49)$$

letting $e_{v_i}(k)$ be the estimation velocity error defined as follows:

$$e_{v_i}(k) = v_i(k) - \hat{v}_i(k), \quad (50)$$

it follows that:

$$e_{v_i}(k) = a_{1i}\hat{v}_i(k-1) + a_{2i}\hat{v}_i(k-2) + b_{1i}i_{Coil}(k-1) + b_{2i}i_{Coil}(k-2) +$$
$$n(k) + c_{1i}n(k-1) + c_{2i}n(k-2), \quad (51)$$

where $\hat{v}_i(k) = \mathcal{Z}^{-1}(\hat{V}_i(z))$, $v_i(k)$ is the real velocity due to the current, coefficients a_{1i}, a_{2i}, b_{1i}, b_{2i} and c_{1i}, c_{2i} are to be estimated, $n(k)$ is assumed to be the white noise. The next sample is:

$$e_{v_i}(k+1) = a_{1i}\hat{v}_i(k) + a_{2i}\hat{v}_i(k-1) + b_{1i}i_{Coil}(k) + b_{2i}i_{Coil}(k-1) +$$
$$n(k+1) + c_{1i}n(k) + c_{2i}n(k-1). \quad (52)$$

The prediction at time "k" is:

$$\hat{e}_{v_i}(k+1/k) = a_{1i}\hat{v}_i(k) + a_{2i}\hat{v}_i(k-1) + b_{1i}i_{Coil}(k) + b_{2i}i_{Coil}(k-1) + c_{1i}n(k) + c_{2i}n(k-1). \quad (53)$$

Considering that:

$$J = E\{e_{v_i}^2(k+1/k)\} = E\{[\hat{e}_{v_i}(k+1/k) + n(k+1)]^2\},$$

and assuming that the noise is not correlated to the signal $\hat{e}_{v_u}(k+1/k)$, it follows:

$$E\{[\hat{e}_{v_i}(k+1/k) + n(k+1)]^2\} = E\{[\hat{e}_{v_i}(k+1/k)]^2\} + E\{[n(k+1)]^2\} = E\{[\hat{e}_{v_i}(k+1/k)]^2\} + \sigma_n^2, \quad (54)$$

where σ_n is defined as the variance of the white noise. The goal is to find $\hat{v}_i(k)$ such that:

$$\hat{e}_{v_i}(k+1/k) = 0. \quad (55)$$

It is possible to write (51) as

$$n(k) = e_{v_i}(k) - a_{1i}\hat{v}_i(k-1) - a_{2i}\hat{v}_i(k-2) - b_{1i}i_{Coil}(k-1) -$$
$$b_{2i}i_{Coil}(k-2) - c_{1i}n(k-1) - c_{2i}n(k-2). \quad (56)$$

Considering the effect of the noise on the system as follows

$$c_{1i}n(k-1) + c_{2i}n(k-2) \approx c_{1i}n(k-1), \quad (57)$$

and using the Z-transform, then:

$$N(z) = \hat{V}_i(z) - a_{1i}z^{-1}\hat{V}_i(z) - a_{2i}z^{-2}\hat{V}_i(z) - b_{1i}z^{-1}I_{Coil}(z) - b_{2i}z^{-2}I_{Coil}(z) - c_{1i}z^{-1}N(z) \quad (58)$$

and

$$N(z) = \frac{(1 - a_{1i}z^{-1} - a_{2i}z^{-2})}{1 + c_{1i}z^{-1}}\hat{V}_i(z) - \frac{(b_{1i}z^{-1} + b_{2i}z^{-2})}{1 + c_{1i}z^{-1}}I_{Coil}(z). \quad (59)$$

The approximation in Eq. (57) is equivalent to consider $\|c_{2i}\| << \|c_{1i}\|$. In other words this position means that a noise model of the first order is assumed. An indirect validation of this assumption is given by the results. In fact, the final measurements show in general good results with the proposed method. Inserting Eq. (59) into Eq. (53) after its Z-transform, and considering positions (57) and (55), the following expression is obtained:

$$\hat{V}_i(z) = -\frac{(a_{1i} + c_{1i} + b_{1i}z^{-1})}{b_{1i}(1 + c_{1i}z^{-1}) + b_{2i}(1 + c_{1i}z^{-1})}I_{Coil}(z). \quad (60)$$

Comparing (60) with (46), it is left with a straightforward diophantine equation to solve. The diophantine equation gives the relationship between the parameters $Y_i = [a_{1i}, b_{1i}, b_{2i}, c_{1i}]$, the parameter k_{app} and the parameters of the system (R_{Coil}, L_{Coil}) as follows:

$$-b_{1i} = k_{app} \quad (61)$$

$$a_{1i} + c_{1i} = k_{app} + t_s\frac{k_{app}C\phi(y(k))}{k_{di}L_{Coil}}k_{pi}R_{Coil} \quad (62)$$

$$b_{1i} + b_{2i} = 1 + t_s\frac{k_{app}}{k_{di}L_{Coil}}C\phi(y(k)) \quad (63)$$

$$b_{1i}c_{1i} + b_{2i}c_{1i} = -1. \quad (64)$$

Considering the estimated velocity signal $\hat{v}_u(t)$ due to the voltage input and with $i_{Coil}(t) = 0$, then it is possible to assume an ARMAX model as follows:

$$v_u(k) = \hat{v}_u(k) + a_{1u}\hat{v}_u(k-1) + a_{2u}\hat{v}_u(k-2) + b_{1u}u_{in}(k-1) + b_{2u}u_{in}(k-2) +$$
$$n(k) + c_{1u}n(k-1) + c_{2u}n(k-2), \quad (65)$$

letting $e_{v_u}(k)$ be the estimation velocity error defined as follows:

$$e_{v_u}(k) = v_u(k) - \hat{v}_u(k), \quad (66)$$

it follows that:

$$e_{v_u}(k) = a_{1u}\hat{v}_u(k-1) + a_{2u}\hat{v}_u(k-2) + b_{1u}u_{in}(k-1) + b_{2u}u_{in}(k-2) +$$
$$n(k) + c_{1u}n(k-1) + c_{2u}n(k-2), \quad (67)$$

where $\hat{v}_u(k) = \mathcal{Z}^{-1}(\hat{V}_u(z))$, $v_u(k)$ is the real velocity due to the input voltage, coefficients a_{1u}, a_{2u}, b_{1u}, b_{2u} and c_{1u}, c_{2u} are to be estimated, $n(k)$ is assumed to be the white noise. The next sample is:

$$e_{v_u}(k+1) = a_{1u}\hat{v}_u(k) + a_{2u}\hat{v}_u(k-1) + b_{1u}u_{in}(k) + b_{2u}u_{in}(k-1) +$$
$$n(k+1) + c_{1u}n(k) + c_{2u}n(k-1). \quad (68)$$

The prediction at time "k" is:

$$\hat{e}_{v_u}(k+1/k) = a_{1u}\hat{v}_u(k) + a_{2u}\hat{v}_u(k-1) + b_{1u}u_{in}(k) + b_{2u}u_{in}(k-1) + c_{1u}n(k) + c_{2u}n(k-1). \quad (69)$$

Considering that:

$$J = E\{e_{v_u}^2(k+1/k)\} = E\{[\hat{e}_{v_u}(k+1/k) + n(k+1)]^2\},$$

and assuming that the noise is not correlated to the signal $\hat{e}_{v_u}(k+1/k)$, it follows:

$$E\{[\hat{e}_u(k+1/k) + n(k+1)]^2\} = E\{[\hat{e}_u(k+1/k)]^2\} + E\{[n(k+1)]^2\} = E\{[\hat{e}_u(k+1/k)]^2\} + \sigma_n^2, \quad (70)$$

where σ_n is defined as the variance of the white noise. The goal is to find $\hat{v}_u(k)$ such that:

$$\hat{e}_u(k+1/k) = 0. \quad (71)$$

It is possible to write (67) as

$$n(k) = e_{v_u}(k) - a_{1u}\hat{v}_u(k-1) - a_{2u}\hat{v}_u(k-2) - b_{1u}u_{in}(k-1) -$$
$$b_{2u}u_{in}(k-2) - c_{1u}n(k-1) - c_{2u}n(k-2). \quad (72)$$

Considering the effect of the noise on the system as follows

$$c_{1u}n(k-1) + c_{2u}n(k-2) \approx c_{1u}n(k-1), \quad (73)$$

and using the Z-transform, then:

$$N(z) = \hat{V}_u(z) - a_{1u}z^{-1}\hat{V}_u(z) - a_{2u}z^{-2}\hat{V}_u(z) - b_{1u}z^{-1}U_{in}(z) - b_{2u}z^{-2}U_{in}(z) - c_{1u}z^{-1}N(z) \quad (74)$$

and

$$N(z) = \frac{(1 - a_{1u}z^{-1} - a_{2u}z^{-2})}{1 + c_{1u}z^{-1}}\hat{V}_u(z) - \frac{(b_{1u}z^{-1} + b_{2u}z^{-2})}{1 + c_{1u}z^{-1}}U_{in}(z). \quad (75)$$

The approximation in Eq. (73) is equivalent to consider $\|c_{2u}\| << \|c_{1u}\|$. In other words this position means that a noise model of the first order is assumed. An indirect validation of this assumption is given by the results. In fact, the final measurements show in general good results with the proposed method. Inserting Eq. (75) into Eq. (69) after its Z-transform, and considering positions (73) and (71), the following expression is obtained:

$$\hat{V}_u(z) = -\frac{(a_{1u} + c_{1u} + b_{1u}z^{-1})}{b_{1u}(1 + c_{1u}z^{-1}) + b_{2u}(1 + c_{1u}z^{-1})}U_{in}(z). \quad (76)$$

Comparing (76) with (47), it is left with a straightforward diophantine equation to solve. The diophantine equation gives the relationship between the parameters $Y_u = [a_{1u}, b_{1u}, b_{2u}, c_{1u}]$, the parameters k_{app}, k_{pu} and the parameters of the system (R_{Coil}, L_{Coil}) as follows:

$$-b_{1u} = 0 \tag{77}$$

$$a_{1u} + c_{1u} = t_s \frac{k_{app} C\phi(y(k))}{k_{di} L_{Coil}} k_{pu} \tag{78}$$

$$b_{1u} + b_{2u} = 1 + t_s \frac{k_{app}}{k_{di} L_{Coil}} C\phi(y(k)) \tag{79}$$

$$b_{1u} c_{1u} + b_{2u} c_{1u} = -1. \tag{80}$$

Procedure:

Heuristic value for parameters k_{app}, k_{di}, k_{pi}, k_{pu} are calculated in order to estimate the state variable according to the desired dynamic performance. This yields initial values for the parameters $Y_i = [a_{1i}, b_{1i}, b_{2i}, c_{1i}]$ and $Y_u = [a_{1u}, b_{1u}, b_{2u}, c_{1u}]$. New values for the vector Y_i and Y_u are calculated using the recursive least squares method with the constraints $b_{1i} c_{1i} + b_{2i} c_{1i} = -1$ and $b_{1u} c_{1u} + b_{2u} c_{1u} = -1$. The technique is described in the following steps:

– **Step 0** Set heuristic values for k_{app}, k_d, and k_p. k_{app} is a big enough value to guarantee the asymptotic approximation of the velocity signal.

– **Step 1**: Calculate the new Y_i, Y_u and parameters of the ARMAX model using the recursive least squares method with the constraints $b_{1i} c_{1i} + b_{2i} c_{1i} = -1$ and $b_{1u} c_{1u} + b_{2u} c_{1u} = -1$.

– **Step 2**: Calculate a new k_{app}, k_{di}, k_{pi}, and k_{pu} from the parameterization of the velocity observer.

– **Step 3**: Calculate the new signals.

– **Step 4**: Update the regressor, $i_{Coil}(k) \rightarrow i_{Coil}(k-1)$, $\hat{v}_i(k-1) \rightarrow \hat{v}_i(k-2)$, $\hat{v}_u(k-1) \rightarrow \hat{v}_u(k-2), \ldots$

Steps 1-4 are repeated for each sampling period.

7. Second-stage of the state observer design: open loop position observer

If the magneto-mechanical part of the system is considered, then

$$\dot{y}(t) = v(t) \tag{81}$$

$$\dot{v}(t) = \frac{f(y(t), i_{Coil}(t))}{m} - \frac{k_v v(t)}{m} - \frac{k_f y(t)}{m}, \tag{82}$$

where $f(y(t), i(t)) = F_{0,max} \sin(2\pi y(t)/d) + k_1 (y(t) + sign(y(t))k_2)i(t)$ as above defined. If the system is written in the following form

$$\left[\begin{array}{c} \dot{y}(t) \\ \dot{v}(t) \end{array}\right] = \left[\begin{array}{cc} 0 & 1 \\ -\frac{k_f}{m} & -\frac{k_v}{m} \end{array}\right] \left[\begin{array}{c} y(t) \\ v(t) \end{array}\right] + \left[\begin{array}{c} 0 \\ \frac{f(y(t),i_{Coil}(t))}{m} \end{array}\right], \tag{83}$$

and if $h(x) = v(t)$, then the observability matrix is the following:

$$\left(O(x_0, u^\star)\right) = \left[\begin{array}{cc} 0 & 1 \\ \frac{F_{0,max}2\pi/d}{m}\cos(2\pi y(t)/d) - \frac{k_f}{m} & -\frac{k_v}{m} \end{array}\right]. \tag{84}$$

Matrix (84) indicates a local uniform observability of the considered system except at the point in which $\cos(2\pi y(t)/d) = \frac{dk_f}{F_{0,max}2\pi}$. This means that, if the velocity is known, then the outputs of the systems are uniformly ($\forall u(t)$) distinguishable except for two isolated points. In fact, according to the data of the developed actuator it results that $dk_f < F_{0,max}2\pi$. Equation (85) is written in the following way:

$$\left[\begin{array}{c} \dot{y}(t) \\ \dot{v}(t) \end{array}\right] = \mathbf{A} \left[\begin{array}{c} y(t) \\ v(t) \end{array}\right] + \left[\begin{array}{c} 0 \\ \frac{f(y(t),i_{Coil}(t))}{m} \end{array}\right], \tag{85}$$

while the output equation

$$v(t) = \left[\begin{array}{cc} 0 & 1 \end{array}\right] \left[\begin{array}{c} y(t) \\ v(t) \end{array}\right] = \mathbf{C} \left[\begin{array}{c} y(t) \\ v(t) \end{array}\right]. \tag{86}$$

It can be clearly seen that $(\mathbf{A}, \mathbf{C})$ is an observable pair, then, according to (Thau (1973)), the observer can be designed as

$$\left[\begin{array}{c} \dot{\hat{y}}(t) \\ \dot{\hat{v}}_L(t) \end{array}\right] = \mathbf{A} \left[\begin{array}{c} \hat{y}(t) \\ \hat{v}_L(t) \end{array}\right] + \left[\begin{array}{c} 0 \\ \frac{f(\hat{y}(t),i_{Coil}(t))}{m} \end{array}\right] + \left[\begin{array}{c} K_y \\ K_v \end{array}\right] (\hat{v}(t) - \hat{v}_L(t)), \tag{87}$$

where $\hat{v}(t) = \mathcal{Z}^{-1}\hat{V}(z)$ calculated above. The corresponding estimation error dynamics are given by

$$\dot{e}(t) = (\mathbf{A} - \mathbf{KC})e(t) + \Delta f(t) = \mathbf{A}_0 e(t) + \Delta f(t), \tag{88}$$

where

$$e(t) = \left[\begin{array}{c} e_y(t) \\ e_v(t) \end{array}\right] = \left[\begin{array}{c} y(t) - \hat{y}(t) \\ v(t) - \hat{v}(t) \end{array}\right], \tag{89}$$

with

$$\mathbf{A}_0 = \mathbf{A} - \mathbf{K}_0 \mathbf{C},$$

$$\mathbf{K}_0 = \left[\begin{array}{c} K_y \\ K_v \end{array}\right],$$

and

$$\Delta f(t) = \left[\begin{array}{c} 0 \\ \frac{f(y(t),i_{Coil}(t))}{m} - \frac{f(\hat{y}(t),i_{Coil}(t))}{m} \end{array}\right].$$

Because of $(\mathbf{A}, \mathbf{C})$ is an observable pair, matrix $\mathbf{A}_0$ for a suitable choice of the observer gain $\mathbf{K}_0$ is a Hurwitz matrix. This yields that there exist symmetric and positive matrices $\mathbf{P}_0$ and $\mathbf{Q}_0$ which satisfy the so called *Lyapunov equation*

$$\mathbf{A}_0^T \mathbf{P}_0 + \mathbf{P}_0 \mathbf{A}_0 = -\mathbf{Q}_0. \tag{90}$$

In order to show the asymptotic stability of (88), the following Lyapunov function is introduced:

$$V(e(t)) = e^T(t)\mathbf{P}_0 e(t). \tag{91}$$

The time derivative is given by

$$\frac{dV(e(t))}{dt} = \dot{e}^T(t)\mathbf{P}_0 e(t) + e^T(t)\mathbf{P}_0 \dot{e}(t) \quad \text{and} \tag{92}$$

from (88) it follows that

$$\frac{dV(e(t))}{dt} = (\mathbf{A}_0 e(t) + \Delta f(t)))^T \mathbf{P}_0 e(t) + e^T(t)\mathbf{P}_0 \dot{e}(t) + e^T(t)\mathbf{P}_0 e(t) + e^T(t)\mathbf{P}_0 (\mathbf{A}_0 e(t) + \Delta f(t))). \tag{93}$$

This yields the following equation:

$$\frac{dV(e(t))}{dt} = (e^T(t)\mathbf{A}_0^T + (\Delta f(t))^T)\mathbf{P}_0 e(t) + e^T(t)\mathbf{P}_0 \dot{e}(t) + e^T(t)\mathbf{P}_0 e(t) + e^T(t)\mathbf{P}_0 (\mathbf{A}_0 e(t) + \Delta f(t))). \tag{94}$$

At the end, considering Eq. (90) it follows that

$$\frac{dV(e(t))}{dt} = (2e^T(t)\mathbf{Q}_0 e(t) + (\Delta f(t))^T \mathbf{P}_0 e(t) + e^t(t)\mathbf{P}_0(\Delta f). \tag{95}$$

Being $\Delta f(t)$ a Lipschitz function, then exists a positive constant L such that, for all points x_1 and x_2 in the domain of the function $\Delta f(t)$

$$\Delta f(x_1, x_2) \le L\|x_1 - x_2\|.$$

If $\lambda_{Q_{0m}}$ is the small eigenvalue of matrix Q_0 and $\lambda_{P_{0M}}$ the biggest eigenvalue of matrix P_0, if

$$\lambda_{Q_{0m}} > \lambda_{P_{0M}}, \tag{96}$$

then

$$\frac{dV(e(t))}{dt} = -2\|\lambda_{Q_{0m}} - L\lambda_{P_{0M}}\|e^2(t). \tag{97}$$

The last equation says that $e(t) = 0$ is an asymptotically stable equilibrium point. The presented demonstration is constrictive in order order to build an observer. In other words, it is enough to choice matrices $\mathbf{K}_0$ and $\mathbf{Q}_0$ such that, through Eq. (90), condition (96) is satisfied.

8. Actuator control

Figure 5 shows the control structure applied to the actuator. The actuator consists of three parts from the control point of view: an electrical system (motor coil), an electromagnetic system (generation reluctance force) and a mechanical system (mass-spring-damper), with the back emf as an internal voltage feedback for the electrical system. Under normal operating conditions, the electrical subsystem is linear and can be represented by the transfer function
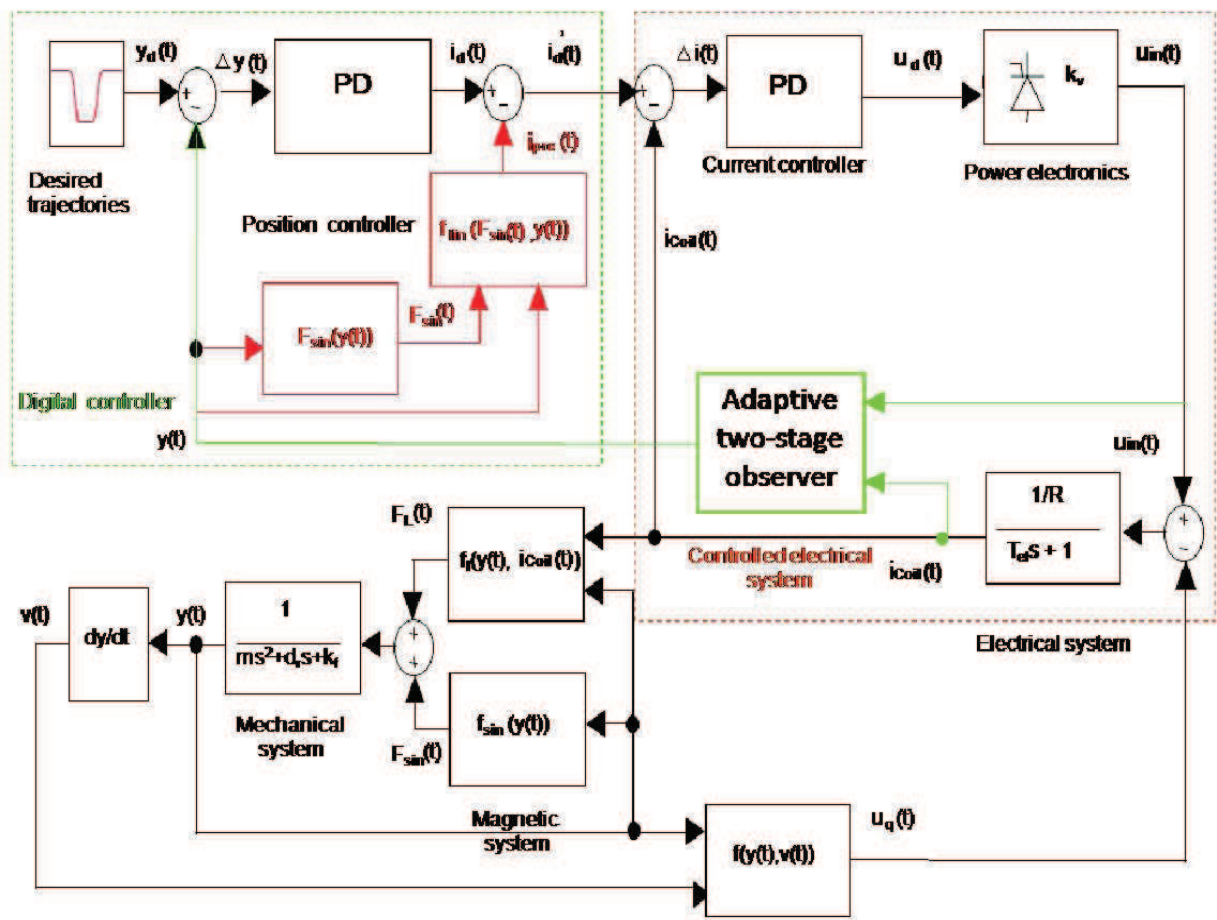
Fig. 5. Control structure

$$G_{el} = \frac{1/R}{Ts + 1} \tag{98}$$

where R is the resistance, and T is the time-constant of the coil. The non-linear electromagnetic force generation can be separated into two parallel blocks, $F_{sin}(y(t))$ and $F_{lin}(y(t), i_{Coil}(t))$ corresponding to the reluctance effect and the Lorentz force, respectively:

$$F(y(t), i_{Coil}(t)) = F_{sin}(y(t)) + F_{lin}(y(t), i_{Coil}(t)), \tag{99}$$

with the following approximative equations

$$
\begin{align}
F_{sin}(y(t)) &= F_{0,max} \sin(2\pi y(t)/d) \quad \text{and} \tag{100} \\
F_{lin}(y(t), i_{Coil}(t)) &= k_1 (y(t) + sign(y(t))k_2) i_{Coil}(t), \tag{101}
\end{align}
$$

where k_1 and k_2 are physical constants. Finally, the mechanical subsystem is characterized by

$$G_m(s) = \frac{Y(s)}{F(s)} = \frac{1}{ms^2 + d_r s + k_f}, \tag{102}$$

with the moving mass m, the viscose damping factor d_r and the spring constant k_f. $Y(s)$ and $F(s)$ are the Laplace transformations of the position $y(t)$ and of the force defined by

Eq. (99) respectively. Because the system damping is very weak, it is obviously up to the control to enable a well-damped overall system. The control structure basically consists of two PD controllers organised in a cascade scheme. PD regulators are often utilised in control problems where a high dynamic range is required. The internal loop is devoted to the current control and provides a compensation of the electrical system, which is the fastest time constant of the physical system. This current controller has an inner loop for back-emf compensation. As the back-emf is difficult to sense, a nonlinear estimator is used for on-line observation. Due to the very high dynamic range required by the valve actuation, the current control loop was realised in an analogue technique, while the trajectory generation and the position control were implemented on a DSP. A common problem of PD-type controllers is the existence of steady-state error. As shown in Fig. 5, a nonlinear feed-forward block, containing the inverse reluctance characteristics, was used to compensate for the nonlinear effects of the actuator and to ensure the stationary accuracy. In fact, having compensated for the nonlinearities, the overall system behaviour can be approximated by a linear third-order system. In particular, the nonlinear compensation is performed while generating the desired current from the inversion of the linear part of the motor characteristic, as described in the following:

$$i_{pre}(t) = \frac{F_{lin}(t)}{k_1(y_d(t) + sign(y_d(t))k_2)}. \tag{103}$$

The inversion of the force-position characteristic of the motor leads to the total actuator force, from which its non-linear part is then subtracted:

$$F_{lin}(t) = ky_d(t) + d\dot{y}_d(t) + m\ddot{y}_d(t) - F_{0,max}\sin(2\pi y_d(t)/d) \tag{104}$$

Finally the following equation is obtained:

$$i_{pre}(t) = \frac{k_f y_d(t) + d_r \dot{y}_d(t) + m\ddot{y}_d(t) - F_{0,max}\sin(2\pi y_d(t)/d)}{k_1(y_d(t) + sign(y_d(t))k_2)}. \tag{105}$$

Based on the desired position signal coming out of the trajectory generator and the measured valve position, a PD-type position controller (lead compensator) is applied. Contrary to the conventional position control in drive systems, where PI-type controllers are mostly used, in this special case we need to increase substantially the exiting phase margin to achieve the desired system damping.

9. Experimental measurements and simulations

The actuator was realised and tested (see the left part of Fig. 6) in our laboratory. Further investigations under real engine conditions were planned. In the right part of Fig. 6, measured reluctance forces for different current densities and armature positions are depicted. Again, the current density was chosen to be -20, -10, 0, 10 or 20 A/mm^2, respectively. Compared to the calculated values the measurements show deviations up to $\sim 8\%$ except for that for the current density of -20 A/mm^2 (here around 13%). The deviation is due to iron saturation, which could not be modelled exactly in the FEM calculation because the material characteristics contained missing data for this region. In other cases, the agreement is obviously better. Here, some typical simulation results using the control structure described above are presented in Fig. 5. The positive effects of the optimised velocity observer are visible in the closed loop control. For the opening phase, a strong but rapidly decreasing gas
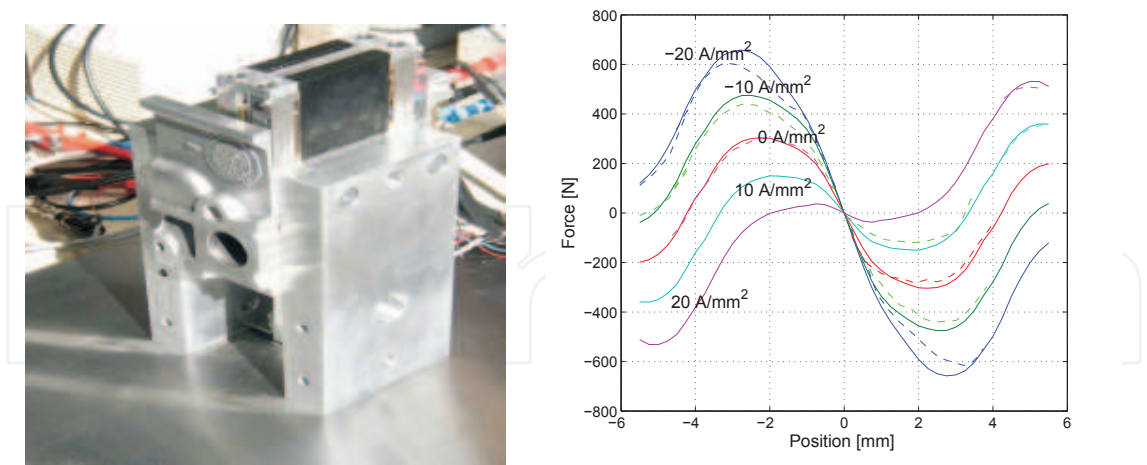
Fig. 6. Left: Actuator experimental set-up. Right: Comparison of calculated and measured characteristic of the motor.
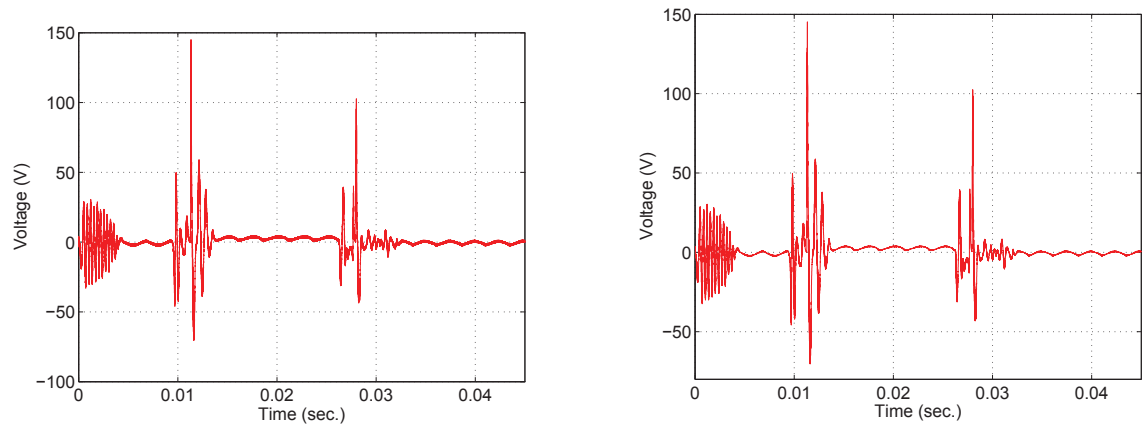

Fig. 7. Left: Closed loop input voltage without optimized observer. Right: Input voltage with optimized observer.
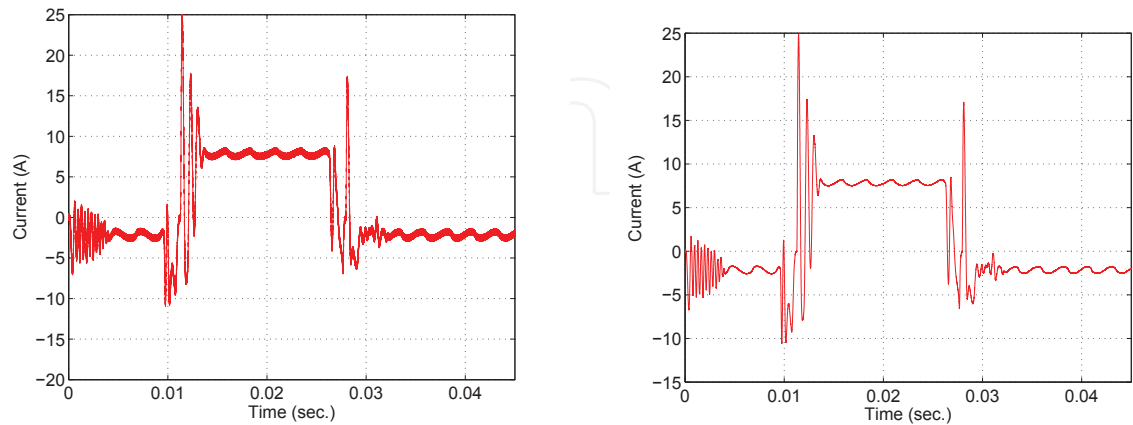

Fig. 8. Left: Closed loop coil current without optimized observer. Right: Coil current with optimized observer.
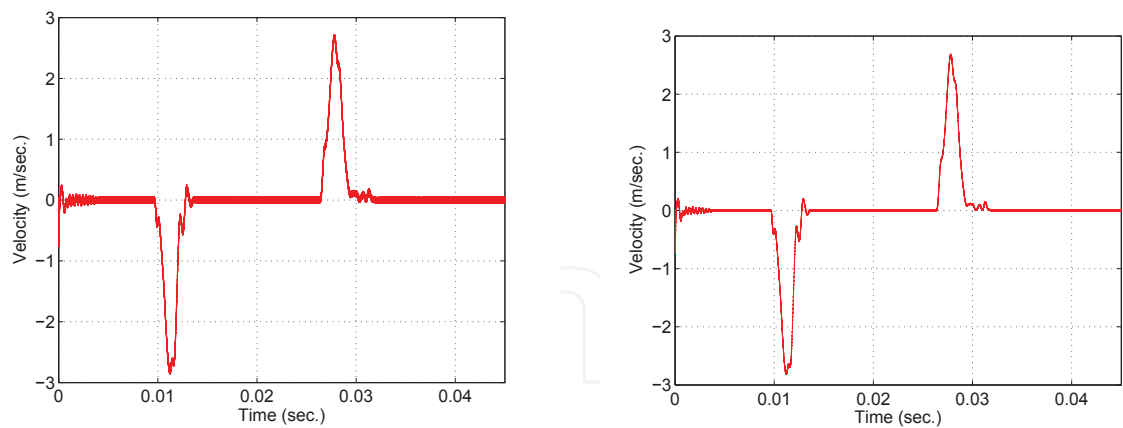
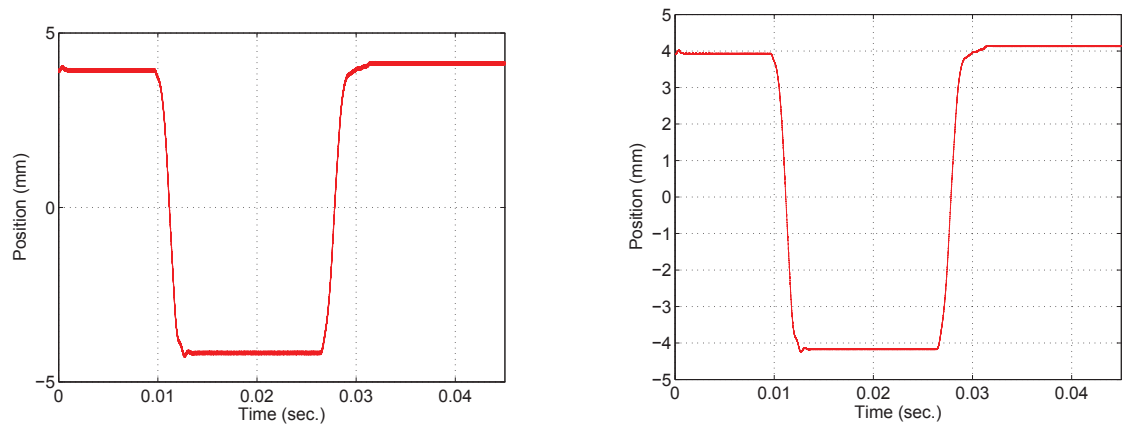Fig. 9. Left: Closed loop velocity without optimized observer. Right: Velocity with optimized observer.

Fig. 10. Left: Closed loop position without optimized observer. Right: Position with optimized observer.

pressure is assumed to be present and is simulated as an unknown disturbance. Even though the presented control strategy does not consider this disturbance condition, the system shows excellent control behaviour. In the simulation, a realistic white noise in the measurement of the current is considered. The typical control behaviour is demonstrated in Fig. 10, where a full-range operation cycle at an engine speed of 3,000 rpm (rounds per minute) is shown. Here, high tracking accuracy is demonstrated, and a reduction of the noise effect is visible. Figure 9 shows also the improvement in the velocity control in the closed loop. The positive effects on the velocity and position control in the closed loop can be justified by the de-noised current and input voltage (see Figs. 8 and 7). Theoretically and in computer simulations, control precision can be further improved by increasing the gain of the controllers. However, measurement noises can cause serious oscillations, which may lead to local stability problems in practical situations.

10. Conclusions and Future Works

The design of a novel linear reluctance motor using permanent-magnet technology is presented. The developed actuator is specifically intended to be used as an electromagnetic engine valve drive. Besides a design analysis, the structure and properties of the applied

An AdaptiveyTwo-Stage Observer in the Control of a
New Electromagnetic Valve Actuator for Camless Internal Combustion Engines

367

control strategy are also discussed. Dynamic simulation results of a sensorless control strategy are presented and show good performance. In particular, based on a nonlinear model, an adaptive two-stage observer is presented that addresses unobservable points and achieves sensorless control. This paper presents feasible real-time self-tuning of an approximated velocity estimator based on measurements of current and input voltage. The robustness of the velocity tracking is addressed using a minimum variance approach. The effect of the noise is minimised, and the position can be achieved through a two-stage structure between this particular velocity estimator and an observer based on the electromechanical system. A control strategy is presented and discussed as well. Computer simulations of the sensorless control structure are presented, in which the positive effects of the optimised velocity observer are visible in the closed-loop control.

10.1 Future Works

Future works could be oriented towards analysis of the stability of the whole closed-loop structure (plant-observer-controller). This analysis could provide useful indications in the determination of the parameters of the PD controller and also in the parameters of the two proposed observers. Future work should also include investigations of further improvements of dynamic range and accuracy using more sophisticated control methods (e.g., sliding-mode control) and experimental measurements under real engine conditions.
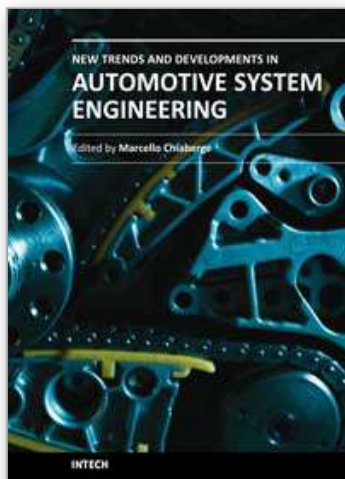
11. Aknowledgement

12. References

Ahmed, T. & Theobald, M.A. (1989). A survey of variable valve actuation technology, In: *SAE Paper (SAE1989)*, SAE, (Ed.), paper number 891674.

Beghi, A., Nardo, L. & Stevanato, M. (2006). Observer-based discrete-time sliding mode throttle control for drive-by-wire operation of a racing motorcycle engine. *Journal Control Systems Technology, IEEE Transactions*, Vol. 14, No. 4, July -2006, pp. 767-775.

Butzmann, S., Melbert, J. & Koch, A. (1989). Sensorless control of electromagnetic actuators for variable valve train, *Proceeding of SAE 2000 World Congress*, paper number 2000-01-1225, Michigan (USA), SAE, (Ed.), Detroit.

Dagci, O.H., Pan, Y. & Ozguner, U. (2002). Sliding mode control of electronic throttle valve, *Proceedings of the 2002 American Control Conference*, pp. 1996-2001, ISBN: 0743-1619, Alaska, 8-10 May 2002 , IEEE, Anchorage.

Furlani, E.P. (2001). *Permanent Magnet and Electromechanical Devices*, Academic Press, USA.

Fabbrini, A., Doretti, D., Braune, S., Garulli, A. & Mercorelli, P. (2008). Optimal trajectory generation for camless internal combustion engine valve control, *Proceedings of of IECON 2008, the 34th Annual Conference of the IEEE Industrial Electronics Society*, pp. 303-308, Florida, 10-13 November 2008 , IEEE, Orlando.

Franklin, G.F., Powell, J.D. & Workman, L.M. (1997). *Digital Control of Dynamic Systems*, Prentice Hall, ISBN-10: 0201820544,USA.

Hermann, R. & Krener, A.J. (1977). Nonlinear controllability and observability, *IEEE Transactions on Automatic Control*, Vol. 22, No. 5, October-1977, pp. 728-740.

Hoffmann, W. & Stefanopoulou, A.G. (2001). Iterative learning control of electromechanical camless valve actuator, *Proceedings of the 2001 American Control Conference*, pp. 2860-2866, ISBN: 0-7803-6495-3, VA (USA), 25-27 June 2001 , IEEE, Arlington.

Kwatny, H.G. & Chang, B.C. (2005). Symbolic computing of nonlinear observable and observer forms, *Applied Mathematics and Computation Elsevier Science Publishing*, Vol. 171, pp. 1058-1080.

Peterson, K.S. (2005). *Control Methodologies for Fast & Low Impact Electromagnetic Actuators for Engine Valves*, PhD Thesis, University of Michigan.

Mercorelli, P. (2009). Robust feedback linearization using an adaptive PD regulator for a sensorless control of a throttle valve, *Mechatronics a journal of IFAC. Elsevier publishing*, Vol. 19, No. 8, November-2009, pp. 1334-1345.

Schlechter, M.M. & Levin, M.B. (1996). Camless engine, In: *SAE Papers (SAE1996)*, SAE, (Ed.), paper number 960581.

Rajamani, R. (1998). Observers for lipschitz nonlinear systems, *IEEE Transactions on Automatic Control*, Vol. 43, No. 3, pp. 397-401.

Slotine, J.J. (1991). *Applied Nonlinear Control*, Ed. Prentice-Hall, ISBN: 0-13-040890-5, Englewood Cliffs, New Jersey (USA).

Tai, C. & Tsao, T. (2003). Control of an electromechanical actuator for camless engines, *Proceedings of the 2001 American Control Conference*, pp. 3113-3118, ISBN: 0-7803-7896-2, Colorado (USA), 4-6 June 2003, IEEE, Denver.

Thau, F.E. (1973). Observing the state of nonlinear dynamic systems, *International Journal of Control*, Vol. 17, No. 3, pp. 471-479.

Wu, R. & Slemon, G.R. (1991). A permanent magnet motor drive without a shaft sensor, *IEEE Transactions on Industrial Applications*, Vol. 27, No. 5, pp. 1005-1011, ISSN: 0093-9994.

Xia, X. & Zeitz, M. (1997). On nonlinear continuous observers, *International Journal of Control*, Vol. 66, No. 6, pp. 943-954.

Zhu, G., Kaddouri, A., Dessaint, L.A. & Akhrif, O. (2001). A nonlinear state observer for the sensorless control of a permanent-magnet AC machine, *IEEE Transactions on Industrial Electronics*, Vol. 48, No. 6, pp. 1098-1108, ISSN: 0278-0046.

New Trends and Developments in Automotive System Engineering
Edited by Prof. Marcello Chiaberge

ISBN 978-953-307-517-4
Hard cover, 664 pages
Publisher InTech
Published online 08, January, 2011
Published in print edition January, 2011

In the last few years the automobile design process is required to become more responsible and responsibly related to environmental needs. Basing the automotive design not only on the appearance, the visual appearance of the vehicle needs to be thought together and deeply integrated with the â€œpowerâ€ developed by the engine. The purpose of this book is to try to present the new technologies development scenario, and not to give any indication about the direction that should be given to the research in this complex and multi-disciplinary challenging field.

INTECH
open science | open minds